Article

Compact LWFA-Based Extreme Ultraviolet Free Electron Laser: Design Constraints

Alexander Yu. Molodozhentsev [ID] and Konstantin O. Kruchinin *[ID]

Institute of Physics ASCR, v.v.i. (FZU), ELI-Beamlines, Za Radnici 835, 25241 Dolni Brezany, Czech Republic; alexander.molodozhentsev@eli-beams.eu

* Correspondence: konstantin.kruchinin@eli-beams.eu

Abstract: The combination of advanced high-power laser technology, new acceleration methods and achievements in undulator development offers the opportunity to build compact, high-brilliance free electron lasers driven by a laser wakefield accelerator. Here, we present a simulation study outlining the main requirements for the laser–plasma-based extreme ultraviolet free electron laser setup with the aim to reach saturation of the photon pulse energy in a single unit of a commercially available undulator with the deflection parameter K_0 in the range of 1–1.5. A dedicated electron beam transport strategy that allows control of the electron beam slice parameters, including collective effects, required by the self-amplified spontaneous emission regime is proposed. Finally, a set of coherent photon radiation parameters achievable in the undulator section utilizing the best experimentally demonstrated electron beam parameters are analyzed. As a result, we demonstrate that the ultra-short, few-fs-level pulse of the photon radiation with the wavelength in the extreme ultraviolet range can be obtained with the peak brilliance of $\sim 7 \times 10^{28}$ photons/pulse/mm^2/mrad^2/0.1%bw.

1. Introduction

In recent years, linac-based free electron lasers (FEL), as a deliverer of coherent X-ray pulses, changed the scientific landscape. Such facilities became an invaluable tool for research in chemistry, biology, material science, medicine and physics [1]. Existing facilities (for example, [2–4]) broaden access to the technology, allowing more researchers to take advantage of the X-ray FEL's unique capabilities. Due to the fact that linac-based X-ray FELs utilize two well-established technologies, conventional or superconducting radio frequency (RF) accelerating structures and permanent magnet-based undulators, such facilities have a total footprint from a few hundred meters (soft X-ray FELs) up to a few kilometers (hard X-ray FELs) and, as a result, are extremely costly. The unique research importance and high cost lead to a situation wherein only a few such facilities operate around the world, with a substantial lack of user-oriented beamtime.

The scientific success and tremendous demand from the photon beam user community stimulate intensive research to find competitive approaches that would lead to a significant size and cost reduction in the instruments. The constantly developing laser wakefield acceleration (LWFA) techniques represent a very attractive candidate for the novel, compact FEL driver [5], especially in light of recent progress in laser technology [6], acceleration gain [7] and breakthroughs in electron beam quality improvement [8].

Over the last decade, the mechanism of the laser–plasma acceleration (LPA) was studied intensively by many groups in order to improve the electron beam parameters by using various LPA schemes, aiming to achieve high-energy, high-quality beams with a sub-percent-level energy spread, low transverse divergence (better than 0.5 mrad RMS), normalized emittances as low as 0.1 π mm mrad and a bunch charge of tens of pC. LPAs have already successfully been applied as undulator-based incoherent light sources [9–13]. A global awareness has been established that LPAs are sufficiently mature as electron beam

drivers for compact coherent light sources from the extreme ultraviolet (EUV) to the soft or even hard X-ray ranges [14,15].

The LPA process creates an electron beam with a transverse divergence that is significantly larger than that of conventional linear accelerators. Such an electron beam has to be focused first by utilizing a set of quadrupole magnets (so-called capture block) placed close to the laser–plasma interaction area. Handling the significant energy spread of the LPA electrons is another problem, which has to be solved intrinsically in the plasma source [16] or by means of the dedicated electron beam transport. A decompression chicane has been proposed [17] to tackle this challenge by applying a controlled rotation of the bunch longitudinal phase space and hence reducing the slice energy spread typical for the LWFA electron beams. In order to produce lasing, the required slice energy spread of the electron bunch passing through the undulator system has to be less than the Pierce parameter, which scales as $\sim 1/\gamma$. It is clear that such a condition is more relaxed in the case of the moderate electron energies (few hundreds of MeV), which in turn restricts the generated photon radiation wavelength to the EUV range. In addition to the slice energy spread, the normalized transverse emittance has to be controlled in order to keep it less than the coherent normalized emittance in the undulator. Finally, the parameters of the electron beam at the entrance of the undulator have to match the undulator Twiss parameters in order to obtain the maximum power of the coherent photon radiation. The undulator Twiss parameters depend on the undulator properties and the focusing structure in the event that a few undulator units are used to reach the FEL saturation regime and produce the high brilliance of the coherent photon radiation.

Recently, the first proof-of-principle demonstration of free electron lasing at 27 nm photon wavelength using three undulator sections driven by a laser wakefield accelerator has been published in [18]. In this experiment, a 490 MeV electron beam was transported using a beamline consisting of a capture block, made by a combination of two permanent and one electromagnetic quadrupole magnets and a matching block made of two electromagnetic quadrupole magnets, used to focus the electron beam into the middle of the 5 m long undulator system. In the above-mentioned work, the electron beam parameters, suitable for lasing, were obtained from the source and no devices for the phase space manipulation were used.

In this paper, we propose a dedicated electron beamline concept where, in addition to the standard three quadrupole-based capture block and an undulator matching, we introduce a new phase space manipulation block consisting of a momentum filter and a decompressor chicane working together as one unit. The momentum filter in this case is used to cut the electron beam halo, caused by the chromatic aberration effects, and serves as a matching for the decompressor, providing a collimated beam, which allows us to avoid a significant increase in the transverse beam size in the chicane. In addition, the proposed electron beamline has enough space to separate the laser and electrons after the laser–plasma interaction, to place dipole correctors and diagnostics to measure the electron bunch properties along the beam transport.

Analysis of the proposed beamline is performed using, as an input, a combination of LWFA electron beam parameters routinely obtained experimentally by various research groups. We show, by means of numerical simulations, that the proposed setup is capable of generating high-brilliance coherent photon radiation in the EUV wavelength range, reaching energy saturation only in the single-unit 3.5 m planar undulator. This offers the opportunity to build compact and cost-effective FEL suitable for user applications with an output peak photon brilliance comparable to the existing linac-based EUV-FEL facilities such as FLASH (Germany) [19] and FERMI (Italy) [20].

2. Main Constraints for a Compact FEL

Aiming to reach saturation of photon energy in one unit, first, the undulator parameters must be fixed. For the purpose of this study, we opted for a very well-developed, commercially available undulator based on hybrid permanent magnet technology with the

deflection parameter $K_0 \sim 1$ designed at "Swiss-FEL" [21]. With this choice, the undulator section length can be defined as no more than 4 m. The main undulator parameters are presented in Table 1.

Table 1. Summary of the undulator, electron beam and FEL parameters.

Parameter	Symbol	Units	Value	
Undulator parameters				
Period	λ_u	mm	15	15
Gap	g_u	mm	4	7
Peak magnetic field	B_0	T	1	0.54
Undulator parameter	K_0	–	1.4	0.75
LWFA-based electron beam parameters				
Energy	W_k	MeV	350	350
RMS emittance (slice)	ε_n	π mm mrad	$<\varepsilon_{coh,n}$	$<\varepsilon_{coh,n}$
RMS beam size in undulator	$<\sigma_{x,y}>$	μm	$\sim$25	$\sim$20
Energy spread (slice)	$\sigma_{\Delta\gamma/\gamma}$	%	0.25	0.25
RMS bunch length	σ_z	μm	1	1
Total bunch charge	Q	pC	25	35
Peak current	I_p	kA	3	4.2
LWFA-based FEL parameters				
Photon radiation wavelength	$\lambda_{ph,1}$	nm	31.6	20.4
Photon radiation energy	$E_{ph,1}$	eV	39	60.5
Coherent RMS emittance	$\varepsilon_{coh,n}$	π mm mrad	1.7	1.2
1D Pierce parameter	ρ_{1D}	–	0.0058	0.0065
1D gain length	$L_{g,1D}$	m	0.12	0.1
1D coherence length	$L_{coh,1D}$	μm	0.4	0.25
Total number of photons at saturation	$N_{photons}$	–	6.2×10^{12}	3.3×10^{12}
Relative FWHM frequency bandwidth	$\delta\lambda_{ph,1}/\lambda_{ph,1}$	%	1.2	1.3
Photon peak brilliance (0.1%BW)	B_{ph}	ph/pulse/mm^2/mrad^2	2.6×10^{29}	3.4×10^{29}
1D peak power at saturation	$P_{ph,1D}$	GW	5.4	5.2
3D gain length	$L_{g,3D}$	m	0.18	0.18
3D total saturation length	$L_{sat,3D}$	m	$\sim$3.5	$\sim$3.5

From the Self-Amplified Spontaneous Emission (SASE) FEL theory [22,23], it is well known that the saturation length of the photon radiation energy is defined by the gain length of the FEL fundamental Gaussian mode and can be expressed as $L_{SAT} \approx 20 \times (1 + \Delta)L_{1D}$. Here, L_{1D} is the gain length determined by one-dimensional FEL theory as a function of basic electron beam and undulator parameters. The Δ-value represents a degradation of the SASE-FEL parameters caused by the finite energy spread, electron beam transverse size and diffraction effect. Taking into account realistic electron beam parameters, reachable in an electron beamline, one can estimate the Δ value to be around 1. Using this constraint, one can conclude that, in order to reach photon energy saturation in a single-unit undulator with a length of less than 4 m, the basic parameters of the electron beam have to be optimized to provide a 1D gain length of no more than 0.1 m.

With the above considerations in mind, an analytic analysis using 1D and 3D SASE-FEL models has been performed assuming Gaussian distribution of electrons in the bunch. The main constraints on the LWFA electron beam and corresponding coherent photon radiation parameters have been derived and are summarized in Table 1. The results indicate that in order to maintain the saturation length of around 3.5 m, the electron beam energy has to be around 350 MeV if the electron bunch, passing through the undulator, has the following parameters: a bunch charge around 25 pC, the RMS transverse size is around 30 μm and the RMS "slice" relative energy spread is around 0.25%. Such energy with stable and reproducible electron beam parameters has been demonstrated experimentally in a compact laser–plasma interaction region [24], utilizing a moderate power of the compressed laser pulse.

Experimental results indicate that an electron beam with sufficient bunch charge and the energy required to operate the FEL in the EUV range can be obtained using a "Joule-class" laser with a pulse duration of $\sim$30 fs. Such lasers are capable of running with

a repetition rate of up to 50 Hz [25], which can boost the average brilliance of the photon radiation to values comparable with the existing RF-based soft X-ray FELs.

3. Laser–Plasma Acceleration for EUV-FEL

Plasma-based accelerators are of great interest because of their ability to sustain extremely large acceleration gradients. The electric field in plasma of the order of 100 GV/m has been demonstrated experimentally [26,27]. Consequently, the accelerating structure required to produce an LWFA electron beam with energy around (300–400) MeV will have the length of a few centimeters. The laser–plasma acceleration technology has made great progress recently to provide a stable operation and produce an electron beam with a peak current of a few kA and energy in the GeV range.

Analyzing the published experimental results obtained by different groups [14], one can identify typical parameters of the electron bunch expected from the LWFA as follows: (1) the normalized transverse root mean square (RMS) emittance of the electron beam is in the range of (0.2–0.5) π μm rad for the electron beam with the peak energy of up to 1 GeV; (2) the RMS transverse divergence is in the range of (0.5–1) mrad; (3) the RMS energy spread with the Full Width at Half Maximum (FWHM) bunch length of a few μm can be reduced down to 1%, keeping the bunch charge of a few tens of pC. The experimentally demonstrated set of LWFA electron bunch initial parameters fits well with the SASE-FEL requirements assuming that one can preserve the electron beam quality while transporting electrons from the LWFA source to the undulator.

4. Electron Beam Transport for EUV-FEL

In order to deliver the LWFA electron beam to an FEL undulator, a dedicated beam transport has to be designed to provide: the capture of electrons from the LWFA source [28]; effective transport of the electron beam with preservation of its quality; possible manipulation with the electron bunch in the longitudinal phase space [17] and, finally, matching the electron beam into the undulator [29]. Moreover, the combination of the significant initial transverse divergence and the large energy spread of LWFA electrons leads to the intrinsic growth of the normalized transverse beam emittance in a drift space after the laser–plasma interaction area [30]. Therefore, the beam transport has to be designed in such a way as to mitigate the emittance growth due to the chromatic effects. Apart from chromatic effects, the laser-driven electron beam, having a bunch duration of a few fs and a bunch charge of a few tens of pC, will suffer from collective effects, which have to be analyzed and taken into account in order to prevent the beam emittance degradation.

The conceptual solution for such beam transport that allows one to reach the SASE-EUV-FEL regime in a single-unit undulator is presented in Figure 1. The proposed beamline consists of the following elements: a capture block, a momentum filter, a decompressor chicane and a matching block.
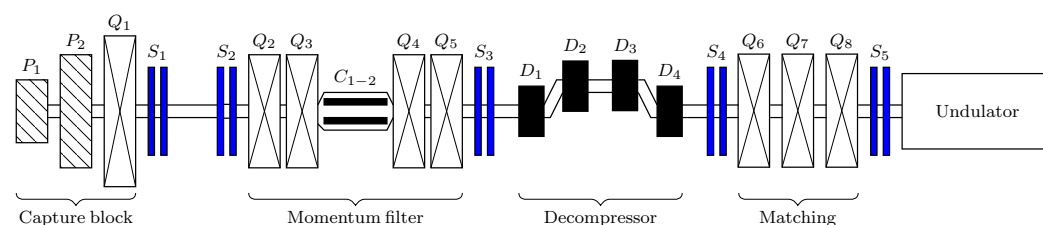

Figure 1. Schematic diagram representing proposed beamline. Here, P_1 and P_2 are permanent quadrupole magnets, Q_1–Q_8 are electromagnetic quadrupoles, C_{1-2} is a pair of horizontal and vertical collimators, S_1–S_5 are pairs of steering magnets (vertical and horizontal) and D_1–D_4 are dipole magnets of the decompressor chicane.

The capture block consists of a pair of Halbach-type permanent quadrupole magnets (PQM) [31] and one conventional electromagnetic quadrupole (EMQ). In spite of a lack of tuning flexibility, PQMs provide the required magnetic field gradient for capturing a

highly divergent electron beam that is unreachable by conventional EMQs. One possible solution to improve the flexibility would be the use of an active plasma lens [32–35] instead of the PQM pair; however, this option needs to be further investigated. As a unit, the capture block has been designed to prevent the growth of the normalized RMS transverse emittance and, at the same time, to focus the electron beam in both planes to propagate through a significant drift space required to separate the driver laser and electron beam after the interaction point.

After passing the first triplet of quadrupoles, the electron beam will form a halo, caused by the chromatic aberrations, leading to the significant degradation of the transverse normalized emittance and, as a result, to the violation of the FEL conditions. To mitigate this issue, a momentum filter [36], consisting of four EMQs with an integrated pair of vertical and horizontal collimators, is placed after the capture block. Inside the momentum filter, the halo particles are effectively filtered out by the collimators. As a result, the projected transverse RMS normalized emittance can be controlled. Optimizing the quadrupole strength of the momentum filter, the almost collimated electron beam can be obtained, which allows for the long drift space required to accommodate the next beamline section.

For the proposed beamline, the aperture of the momentum filter collimators (C_{MF}) was set to 430 μm. An additional collimator (C_U) with the aperture of 620 μm was placed in front of the undulator entrance in order to clean the beam halo and control the slice normalized transverse emittance, as required by the SASE-FEL regime.

The normalized transverse emittance of the electron bunch after the momentum filter, as well as the particle losses at the C_{MF}-collimator, depend on the initial energy spread of the electrons in the bunch. In the case of the initial RMS energy spread of 1% and the open C_{MF}-collimator, the normalized RMS transverse emittance after the momentum filter is 1.5 π mm mrad. For the same initial energy spread, the normalized RMS emittance becomes less than 0.6 π mm mrad with just 13% of the particle losses if the C_{MF}-collimator has the aperture of 430 μm. If no space charge effects are present, only 7% of the electrons in the bunch will be lost in this case. Total losses after all sections of the beamline are around 20%. Losses along the beamline are presented on the bottom plot in Figure 2.
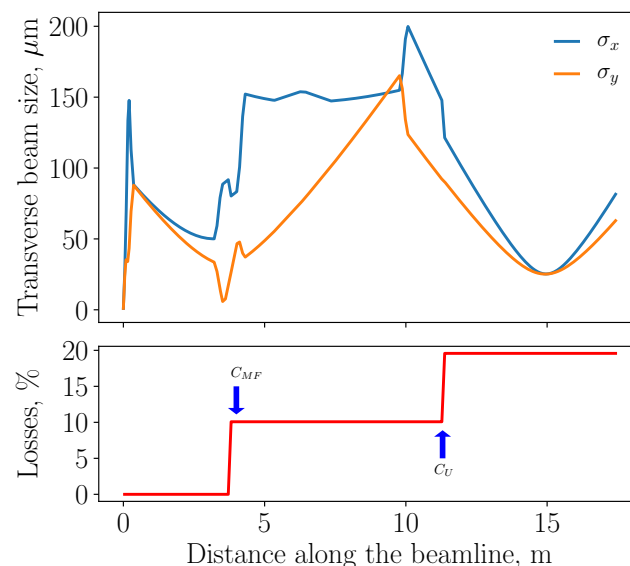

Figure 2. Simulated electron beam horizontal and vertical envelopes (top) and beam losses (bottom) along the beamline. Arrows on the bottom plot show the position of the momentum filter collimator (C_{MF}) and collimator before the undulator entrance (C_U). Parameters: electron energy is 350 MeV, decompressor bending angle is 0.35 deg, initial bunch charge is 45 pC. The center of the single-unit undulator is located at 15 m from the source.

As mentioned previously, the LWFA electron beam has a relatively large (compared to the conventional RF accelerators) initial energy spread, which makes it impossible to reach the FEL regime. As proposed in [17], this problem can be solved by introducing a dispersive section (a decompressor chicane) into the beamline, where the electron bunch is stretched longitudinally and effectively sorted by energy, resulting in a reduction in the local (slice) energy spread at the cost of a reduced peak current and an energy chirp. The slice energy spread in this case can be controlled by adjusting the bending angle of the chicane dipole magnets. For the proper optimization of the magnetic chicane performance, the space charge effect at low electron energy has to be taken into account. The space charge force will change the transverse and longitudinal particle distribution in the bunch, leading to an almost uniform longitudinal beam profile.

The result of such optimization is presented in Figure 3, showing variation in the FWHM bunch length and the average slice RMS energy spread as a function of the decompressor bending angle for various bunch charges. The slice length is determined by the coherence length for the SASE-FEL regime. The required slice energy spread is defined by the SASE-FEL constraints discussed above. In order to keep the slice energy spread below 0.25%, dictated by the FEL study described in the previous section, the bending angle of the decompressor has to be no less than 0.35 degrees and the initial projected RMS energy spread of the electron bunch has to be 0.5%. Further increase in the angle will lead to a peak current reduction. To keep the current at the same level, more charge is required. Increasing the charge will intensify the collective effects, which, at some point, will lead to the degradation of the electron beam quality [37].
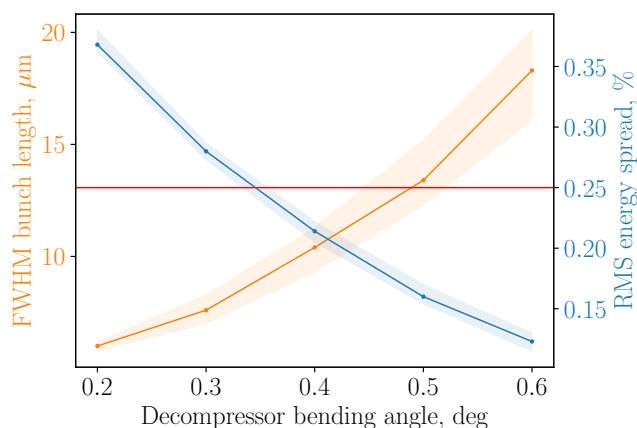

Figure 3. FWHM bunch length (orange) and slice RMS energy spread (blue) as a function of the decompressor bending angle. The solid lines represent the case for the bunch charge of 35 pC. Shaded areas represent the bunch charge variation in the range of (25–45) pC. The initial projected RMS energy spread is equal to 0.5%.

Finally, the matching block consisting of three EMQs is placed before the undulator. This block allows us to focus the electron beam to the required transverse dimension, both vertically and horizontally, in the middle of the undulator.

In addition to the described beam transport sections, sufficient drift space has to be reserved between blocks in order to place steering magnets for the orbit correction and various beam diagnostic devices [38].

The electron beam dynamics for the proposed beamline have been studied using the TraceWin code [39], taking into account the space charge effect in combination with the collimation of the beam. Initial electron beam parameters were optimized to provide the required slice electron beam parameters presented in Table 1. An example of the transverse beam size variation along the beamline is presented in Figure 2. In this case, the initial projected RMS energy spread is equal to 0.5%, the RMS transverse divergence of the electron beam is 0.5 mrad, the RMS bunch length is 1 μm and the total bunch charge is 40 pC. As one can see, the proposed beam transport design allows us to focus

the beam down to ∼25 μm in both planes, with propagation efficiency of approximately 80%, keeping the normalized RMS projected emittance at the level of 0.6 π mm mrad at the entrance of the undulator. Proper optimization of the decompressor chicane allows us to keep the slice energy spread below 0.25% and the slice RMS normalized transverse emittance no more than 0.4 π mm mrad, as required to achieve the FEL performance.

The simulated transverse and longitudinal phase spaces are presented in Figure 4, representing the bunch behavior along the electron beamline. The decompression chicane leads to a significant reduction in the slice energy spread (Figure 4 images (l) and (o)), inducing an additional energy chirp. The length of the slice is determined by the FEL coherence length, which is less than 0.5 μm (see Table 1). The average energy of each longitudinal slice will be slightly different. This will lead to the variation in the photon wavelength generated by each individual slice. Nevertheless, the resulting variation in the wavelength remains less than the fundamental broadening, which is mainly defined by the Pierce parameter. In this case, the energy chirp introduced by the decompressor chicane will not be noticeable in the EUV wavelength region.
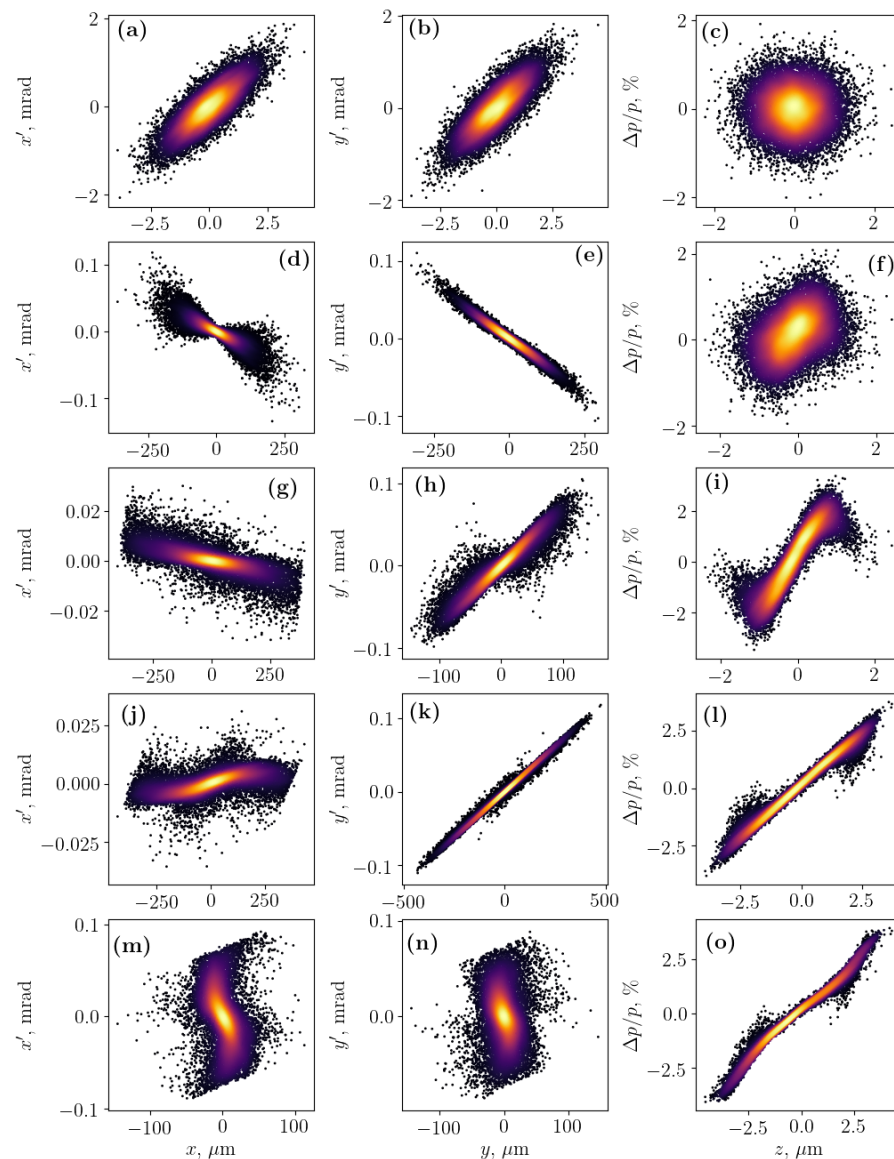

Figure 4. Simulated transverse and longitudinal phase space projections after each beamline section: after the source (**a–c**), after the capture block (**d–f**), after the momentum filter (**g–i**), after the decompressor (**j–l**) and in the middle of the undulator (**m–o**).

5. EUV-FEL Regime

The start-to-end simulations of the electron beam dynamics with collective effects and the generation of the coherent photon radiation in the chosen undulator have been performed by using the optimized set of the decompressor chicane. The SASE-FEL regime in the case of a single-unit undulator with the gap size of 4 mm has been studied, using the SIMPLEX code [40], to confirm the saturation of the radiation power at the exit of the undulator, including an external seeding to improve the longitudinal coherence of the generated photon pulse.

The results of the study are presented in Figures 5 and 6, showing photon energy amplification inside the undulator and the corresponding energy spectrum, respectively. As one can notice, the saturation of the photon pulse energy can be reached after approximately 3.5 m if the initial projected RMS energy spread of the laser-driven electron beam is 0.5%. The corresponding value of the radiation peak brilliance is 7.5×10^{28} photons/pulse/mrad^2/mm^2/0.1%bw. If the initial projected RMS energy spread is increased to 1%, the saturation of the photon pulse energy along the same undulator cannot be obtained.
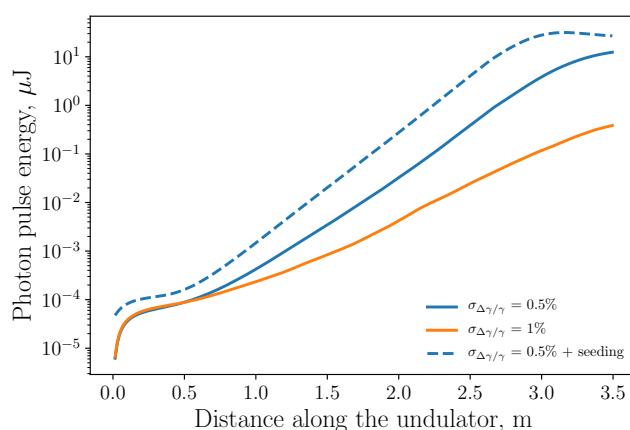

Figure 5. Photon pulse energy amplification for different projected energy spread in the case of the optimized decompressor angle.

An external seeding with proper parameters allows us to reduce the saturation length and increase the photon pulse energy. In the case of the EUV-FEL, the direct seeding by the high harmonic generation (HHG) in noble gases [41] can be used. The seeding signal can be obtained from the main laser pulse used for the electron acceleration. This approach will simplify the required synchronization between the electron beam and the seeding signal at the entrance of the undulator.

To demonstrate this, an external signal with a wavelength of 31.6 nm and power of 1.2 kW was applied in the simulation to the case of 0.5% initial energy spread. The photon radiation energy saturation in this case can be reached after around 3 meters, producing a single-spike energy spectrum.

The photon radiation wavelength can be tuned by varying the undulator gap. An example of the output parameters for the gap size of 7 mm is presented in Table 1. It must be taken into account that, for each gap position, the electron peak current and consequently all the beamline parameters have to be re-optimized in order to reach the saturation of the photon energy at the fixed undulator length.
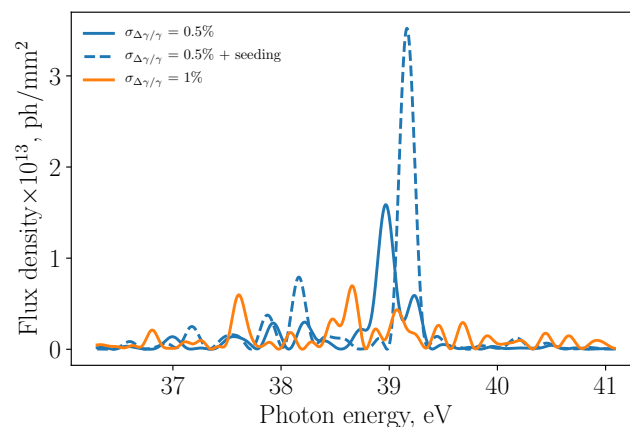
Figure 6. Flux density in units of number of photons/pulse/mm^2 per the energy bandwidth of 0.1% without (solid line) and with external seeding (dashed line).

6. Conclusions

A comprehensive analysis of the LWFA electron beam main parameters has been performed in order to provide the saturation of the photon energy in the single-unit "Swiss-FEL"-type undulator. It was shown that the LWFA electron beam with the energy of 350 MeV is capable of generating a fundamental harmonic photon radiation with a wavelength in the range of (20.4–31.6) nm depending on the undulator gap size. A dedicated electron beam transport has been presented, allowing us to deliver the electron beam from the LWFA source to the FEL undulator with the parameters needed to reach saturation of the photon radiation power in the EUV wavelength range in a single undulator unit with a length of less than 4 m.

Is was demonstrated that the saturation of the photon radiation power can be reached at the end of the single-unit "Swiss-FEL"-type undulator, even without additional external seeding after the optimization of the electron beam slice parameters. The proper seeding signal allows us to reduce the saturation length and generate a photon energy spike with improved longitudinal coherence. The peak brilliance of the single-spike photon radiation with the wavelength of ∼31.6 nm was found to be ∼7.5×10^{28} photon/pulse/mrad^2/mm^2/0.1%bw. Combination of the laser-driven FEL development with novel high-power, high-repetition rate laser technology will introduce a new perspective in the development of compact soft X-ray FELs with few or even sub-femtosecond photon bunches for a very wide user community.

Institutional Review Board Statement: Not Applicable.

Informed Consent Statement: Not Applicable.

Data Availability Statement: The data supporting presented study are available from the corresponding author upon reasonable request.

Conflicts of Interest: The authors declare no conflicts of interest.

References

1.　Pellegrini, C. The development of XFELs. *Nat. Rev. Phys.* **2020**, *2*, 330–331. [CrossRef]
2.　*XFEL: The European X-Ray Free-Electron Laser. Technical Design Report*; DESY: Hamburg, Germany,2006. [CrossRef]
3.　Milne, C.J.; Schietinger, T.; Aiba, M.; Alarcon, A.; Alex, J.; Anghel, A.; Arsov, V.; Beard, C.; Beaud, P.; Bettoni, S.; Bopp, M.; et al. SwissFEL: The Swiss X-ray Free Electron Laser. *Appl. Sci.* **2017**, *7*, 720. [CrossRef]
4.　Huang, Z.; Lindau, I. SACLA hard-X-ray compact FEL. *Nat. Photonics* **2012**, *6*, 505–506. [CrossRef]
5.　Gruner, F.; Becker, S.; Schramm, U.; Eichner, T.; Fuchs, M.; Weingartner, R.; Habs, D.; Meyer-ter-Vehn, J.; Geissler, M.; Ferrario, M.; et al. Design considerations for table-top, laser-based VUV and X-ray free electron lasers. *Appl. Phys. B* **2007**, *86*, 431–435. [CrossRef]
6.　Mourou, G.; Tajima, T. The Extreme Light Infrastructure: Optics' Next Horizon. *Opt. Photon. News* **2011**, *22*, 47–51. [CrossRef]
7.　Gonsalves, A.; Nakamura, K.; Daniels, J.; Benedetti, C.; Pieronek, C.; de Raadt, T.; Steinke, S.; Bin, J.; Bulanov, S.; van Tilborg, J.; et al. Petawatt Laser Guiding and Electron Beam Acceleration to 8 GeV in a Laser-Heated Capillary Discharge Waveguide. *Phys. Rev. Lett.* **2019**, *122*, 084801. [CrossRef] [PubMed]
8.　Jalas, S.; Kirchen, M.; Messner, P.; Winkler, P.; Hübner, L.; Dirkwinkel, J.; Schnepp, M.; Lehe, R.; Maier, A.R. Bayesian Optimization of a Laser-Plasma Accelerator. *Phy. Rev. Lett.* **2021**, *126*, 505–506. [CrossRef]
9.　Schlenvoigt, H.P.; Haupt, K.; Debus, A.; Budde, F.; Jäckel, O.; Pfotenhauer, S.; Schwoerer, H.; Rohwer, E.; Gallacher, J.G.; Brunetti, E.; et al. A compact synchrotron radiation source driven by a laser-plasma wakefield accelerator. *Nat. Phys.* **2008**, *4*, 130–133. [CrossRef]
10.　Fuchs, M.; Weingartner, R.; Popp, A.; Major, Z.; Becker, S.; Osterhoff, J.; Cortrie, I.; Zeitler, B.; Hörlein, R.; Tsakiris, G.D.; et al. Laser-driven soft-X-ray undulator source. *Nat. Phys.* **2009**, *5*, 826–829. [CrossRef]
11.　André, T.; Andriyash, I.A.; Loulergue, A.; Labat, M.; Roussel, E.; Ghaith, A.; Khojoyan, M.; Thaury, C.; Valléau, M.; Briquez, F.; et al. Control of laser plasma accelerated electrons for light sources. *Nat. Commun.* **2018**, *9*, 1334. [CrossRef]
12.　Delbos, N.; Werle, C.; Dornmair, I.; Eichner, T.; Hübner, L.; Jalas, S.; Jolly, S.; Kirchen, M.; Leroux, V.; Messner, P.; et al. Lux—A laser-plasma driven undulator beamline. *Nucl. Instrum. Methods Phys. Res. Sect. Accel. Spectrometers Detect. Assoc. Equip.* **2018**, *909*, 318–322. [CrossRef]
13.　Maier, A.R.; Kajumba, N.; Guggenmos, A.; Werle, C.; Wenz, J.; Delbos, N.; Zeitler, B.; Dornmair, I.; Schmidt, J.; Gullikson, E.M.; et al. Water-Window X-Ray Pulses from a Laser-Plasma Driven Undulator. *Sci. Rep.* **2020**, *10*, 5634. [CrossRef]
14.　Assmann, R.W.; Weikum, M.K.; Akhter, T.; Alesini, D.; Alexandrova, A.S.; Anania, M.P.; Andreev, N.E.; Andriyash, I.; Artioli, M.; Aschikhin, A.; et al. EuPRAXIA Conceptual Design Report. *Eur. Phys. J. Spec. Top.* **2020**, *229*, 3675–4284. [CrossRef]
15.　Ghaith, A.; Couprie, M.E.; Oumbarek-Espinos, D.; Andriyash, I.; Massimo, F.; Clarke, J.; Courthold, M.; Bayliss, V.; Bernhard, A.; Trunk, M.; et al. Undulator design for a laser-plasma-based free-electron-laser. *Phys. Rep.* **2021**, *937*, 1–73. [CrossRef]
16.　Zhang, Z.; Li, W.; Liu, J.; Wang, W.; Yu, C.; Tian, Y.; Nakajima, K.; Deng, A.; Qi, R.; Wang, C.; et al. Energy spread minimization in a cascaded laser wakefield accelerator via velocity bunching. *Phys. Plasmas* **2016**, *23*, 053106. [CrossRef]
17.　Maier, A.R.; Meseck, A.; Reiche, S.; Schroeder, C.B.; Seggebrock, T.; Gruener, F. Demonstration Scheme for a Laser-Plasma-Driven Free-Electron Laser. *Phys. Rev. X* **2012**, *2*, 031019. [CrossRef]
18.　Wang, W.; Feng, K.; Ke, L.; Yu, C.; Xu, Y.; Qi, R.; Chen, Y.; Qin, Z.; Zhang, Z.; Fang, M.; et al. Free-electron lasing at 27 nanometres based on a laser wakefield accelerator. *Nature* **2021**, *595*, 516–520. [CrossRef]
19.　Faatz, B.; Braune, M.; Hensler, O.; Honkavaara, K.; Kammering, R.; Kuhlmann, M.; Ploenjes, E.; Roensch-Schulenburg, J.; Schneidmiller, E.; Schreiber, S.; et al. The FLASH Facility: Advanced Options for FLASH2 and Future Perspectives. *Appl. Sci.* **2017**, *7*, 1114. [CrossRef]
20.　Bocchetta C.; Abrami A.; Allaria E.; Andrian I.; Bacescu D.; Badano L.; Banchi L.; Bulfone D.; Bonțoiu C.; Bracco R.; et al. *Conceptual Design Report for the FERMI@Elettra Project*; ST/F-TN-07/12; Elettra Sincrotrone Trieste: Basovizza, Italy. 2007.
21.　Schmidt, T.; Böhler, P.; Brügger, M.; Calvi, M.; Danner, S.; Huber, P.; Imhof, A.; Jöhri, H.; Keller, A.; Locher, M.; et al. SwissFEL U15 prototype design and first results. In *Proceedings of Free Electron Laser Conference (IBIC'12)*; JACoW Publishing: Geneva, Switzerland, 2012; pp. 666–669.
22.　Xie, M. Exact and variational solutions of 3D eigenmodes in high gain FELs. *Nucl. Instrum. Methods Phys. Res. A* **2000**, *445*, 59–66. [CrossRef]
23.　Huang, Z.; Kim, K.J. Review of x-ray free-electron laser theory. *Phys. Rev. ST Accel. Beams* **2007**, *10*, 034801. [CrossRef]
24.　Maier, A.R.; Delbos, N.M.; Eichner, T.; Hübner, L.; Jalas, S.; Jeppe, L.; Jolly, S.W.; Kirchen, M.; Leroux, V.; Messner, P.; et al. Decoding Sources of Energy Variability in a Laser-Plasma Accelerator. *Phys. Rev. X* **2020**, *10*, 031039. [CrossRef]
25.　Green, T.; Antipenkov, R.; Bakule, P. L2-DUHA 100TW High Repetition Rate Laser System at ELI-Beamlines: Key Design Considerations. *Rev. Laser Eng.* **2021**, *49*, 106–109.
26.　Malka, V.; Fritzler, S.; Lefebvre, E.; Aleonard, M.-M.; Burgy, F.; Chambaret, J.-P.; Chemin, J.-F.; Krushelnick, K.; Malka, G.; Dangor, A.E.; et al. Electron Acceleration by a Wake Field Forced by an Intense Ultrashort Laser Pulse. *Science* **2002**, *298*, 1596–1600. [CrossRef] [PubMed]
27.　Hafz, N.A.M.; Jeong, T.M.; Choi, I.W.; Lee, S.K.; Pae, K.H.; Kulagin, V.V.; Sung, J.H.; Yu, T.J.; Hong, K.-H.; Hosokai, T.; et al. Electron stable generation of GeV-class electron beams from self-guided laser-plasma channels. *Nature* **2008**, *2*, 571–577. [CrossRef]

28. Hofmann, I. Halo coupling and cleaning by a space charge resonance in high intensity beams. *Phys. Rev. ST Accel. Beams* **2013**, *16*, 084201. [CrossRef]

29. Loulergue; Labat, A.; Evain, M.; Benabderrahmane, C.; Malka, C.; Couprie, E.M. Beam manipulation for compact laser wakefield accelerator based free-electron lasers. *New J. Phys.* **2015**, *17*, 023028. [CrossRef]

30. Migliorati, M.; Bacci, A.; Benedetti, C.; Chiadroni, E.; Ferrario, M.; Mostacci, A.; Palumbo, L.; Rossi, A.R.; Serafini, L.; Antici, P. Intrinsic normalized emittance growth in laser-driven electron accelerators. *Phys. Rev. ST Accel. Beams* **2013**, *16*, 011302. [CrossRef]

31. Halbach, K. Design of permanent multipole magnets with oriented rare earth cobalt material. *Nucl. Instrum. Methods* **1980**, *169*, 1–10. [CrossRef]

32. Panofsky, W.K.H.; Baker, W.R. A Focusing Device for the External 350-MeV Proton Beam of the 184-inch Cyclotron at Berkeley. *Rev. Sci. Instrum.* **1950**, *21*, 445–447. [CrossRef]

33. Chiadroni, E.; Anania, M.; Bellaveglia, M.; Biagioni, A.; Bisesto, F.; Brentegani, E.; Cardelli, F.; Cianchi, A.; Costa, G.; Di Giovenale, D.; et al. Overview of plasma lens experiments and recent results at SPARC_LAB. *Nucl. Instrum. Methods Phys. Res. A* **2018**, *909*, 16–20. [CrossRef]

34. van Tilborg, J.; Barber, S.K.; Benedetti, C.; Schroeder, C.B.; Isono, F.; Tsai, H.E.; Geddes, C.G.R.; Leemans, W.P. Comparative study of active plasma lenses in high-quality electron accelerator transport lines. *Phys. Plasmas* **2018**, *25*, 056702. [CrossRef]

35. Lindstrøm, C.; Sjobak, K.; Adli, E.; Röckemann, J.H.; Schaper, L.; Osterhoff, J.; Dyson, A.; Hooker, S.; Farabolini, W.; Gamba, D.; Corsini, R. Overview of the CLEAR plasma lens experiment. *Nucl. Instrum. Methods Phys. Res. A* **2018**, *909*, 379–382. [CrossRef]

36. Molodozhentsev, A.; Korn, G.; Maier, A.; Pribyl, L. "LWFA-driven" Free Electron Laser for ELI-Beamlines. In Proceedings of the 60th ICFA Advanced Beam Dynamics Workshop (FLS'18), Shanghai, China, 5–9 March 2018; JACoW Publishing: Geneva, Switzerland, 2018; pp. 62–67.

37. Molodozhentsev, A.; Kruchinin, K.; Pribyl, L. Degradation of Electron Beam Quality for a Compact Laser-Based FEL. In Proceedings of the 9th International Particle Accelerator Conference (IPAC'18), Vancouver, BC, Canada, 29 April–4 May 2018; JACoW Publishing: Geneva, Switzerland, 2018; pp. 3029–3031. Conference. [CrossRef]

38. Kruchinin, K.; Kocon, D.; Lyapin, A. Electron Beam Diagnostics Concept for the LWFA Driven FEL at ELI-Beamlines. *Proc. IBIC* **2019**, *19*, 184–187. [CrossRef]

39. Uriot, D.; Pichoff, N. Status of TraceWin Code. In Proceedings of the 6th International Particle Accelerator Conference (IPAC'15), Richmond, VA, USA, 3–8 May 2015; JACoW: Geneva, Switzerland, 2015; pp. 92–94.

40. Tanaka, T. *SIMPLEX*: Simulator and postprocessor for free-electron laser experiments. *J. Synchrotron Radiat.* **2015**, *22*, 1319–1326. [CrossRef] [PubMed]

41. Reiche, S. Overview of seeding methods for FELs. In Proceedings of the 4th International Particle Accelerator Conference (IPAC'13), Shanghai, China, 12–17 May 2013; JACoW Publishing: Geneva, Switzerland; pp. 2063–2067.